

AURORAL IMAGES AND PARTICLE PRECIPITATIONS
OBSERVED BY THE SOUNDING ROCKET
EXPERIMENT AT SYOWA STATION

Masaki EJIRI¹, Takeo HIRASAWA¹, Takayuki ONO¹
and Takasi OGUTI²

¹National Institute of Polar Research,
9-10, Kaga 1-chome, Itabashi-ku, Tokyo 173

²Geophysics Research Laboratory, University of Tokyo,
3-1, Hongo 7-chome, Bunkyo-ku, Tokyo 113

Abstract: Three sounding rockets were launched in 1984 from Syowa Station in Antarctica into different types of aurora, designated as AURORA I (an active auroral arc at the substorm expansion phase), II (a stable arc prior to the substorm onset) and III (a diffuse aurora during the recovery phase). A new low-light-level television camera was also used to take an auroral picture downwards from the spinning rocket, together with the electrostatic quadrispherical and magnetic electron spectrometers to measure the energy spectrum of auroral particles (electrons). AURORA I showed greater values in both auroral emission and electron density than for AURORA II. AURORA III, although the auroral emission intensity was much less of course in comparison with AURORA I, the electron density showed a pronounced enhancement in the *D* region and was comparable with the case of AURORA I above the *E* region. The electron temperature for the three cases do not differ so much and are quite similar with one another below 150 km in altitude.

As for an energy spectrum of auroral electrons, AURORA I and II showed an inverted-V type monoenergetic peak with much greater energy for AURORA I than for AURORA II, whereas AURORA III exhibits a power-law spectrum with a small superposing monoenergetic peak around 0.5 keV above 200 km in altitude. A differential energy flux of trapped electrons is generally greater than that of precipitating electrons.

The television camera data taken from the rocket showed a dependence of auroral color spectrum on the auroral activity, *i.e.*, the ratio of an apparent emission rate at 427.8 nm and an illuminance in a visible range (400 to 800 nm) becomes greater for brighter aurora.

1. Introduction

Auroral particle precipitations along the geomagnetic field have been recognized by the electron detectors on board the polar orbiting satellite OGO 4 (HOFFMAN and EVANS, 1968; HOFFMAN, 1969), and HEIKKILA (1970) found pronounced peaks in the particle energy spectrum obtained by a soft particle spectrometer of the ISIS satellite. Using the Injun 5 satellite FRANK and ACKERSON (1971) examined the energy-time (*E-t*) spectra of precipitating particles, which showed a persistent "inverted-V substructure" in the auroral zone. The rocket-borne detectors also clarified the unique energy spectra of precipitating auroral electrons and their back-scattered (upward)

particles (ARNOLDY and CHOY, 1973; ARNOLDY *et al.*, 1974). With the Atmosphere Explorer D (AE-D) satellite detailed characteristics of inverted-V events have been investigated (LIN and HOFFMAN, 1979a, b; HOFFMAN and LIN, 1981) and their small scale structures are identified to be related to auroral arcs (LIN and HOFFMAN, 1982). THIEMAN and HOFFMAN (1985) compared the inverted-V events observed by two Dynamic Explorer spacecraft (DE-1 and -2) at close proximity locations with different altitudes.

Characteristics of inverted-V structure of precipitating auroral particles suggest a source acceleration mechanism which implies a potential drop along the geomagnetic field line, and several theoretical and observational investigations have been presented (see an extensive review by AKASOFU and KAN, 1981; PULLIAM *et al.*, 1981; MENIETTI and BURCH, 1981; STASIEWICZ, 1985; LOTKO, 1986).

There are distinctly three different types of auroras during the course of polar geomagnetic disturbance, that is, a pre-breakup stable arc, an active auroral arc at the expansion phase of substorm, and a diffuse aurora during the recovery phase. The energy spectra of auroral particles and images of auroral emissions have been observed together with electron density and temperature profiles by three sounding rockets flown into the above-mentioned three different types of auroras, a preliminary result of which was presented earlier by NAGATA *et al.* (1985). This paper gives the detailed results of comprehensive analysis obtained by the three rocket experiments.

2. Instrumentation

The sounding rocket experiment at the 25th Japanese Antarctic Research Ex-

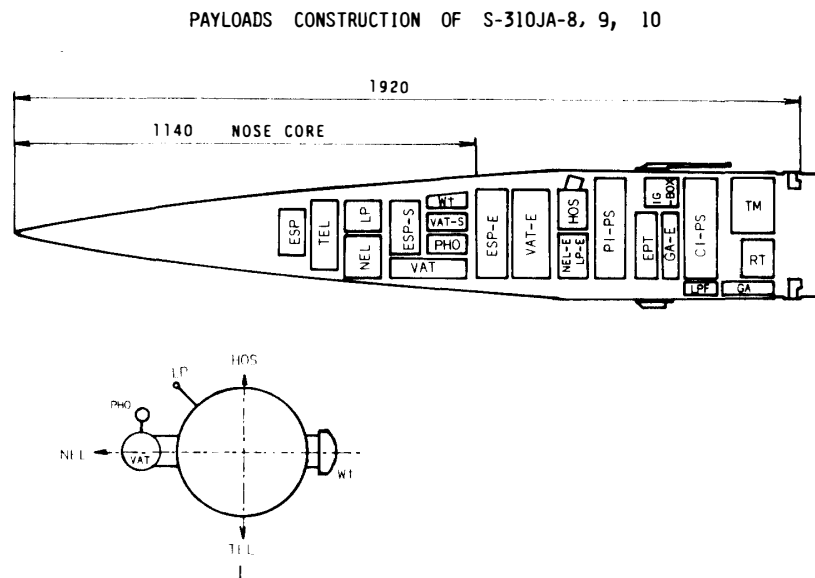


Fig. 1. Payload construction of the sounding rocket. As for each scientific instrument, see text. E stands for electronics, S a sensor, PS a power supply, PI a payload, CI common instruments such as TM (a telemetry instrument) and RT (a radar transponder), IG an igniter, and LPF a low pass filter. The dimension is in mm. The rocket diameter is 310 mm.

pedition (wintering in 1984) was planned to investigate the causality between auroral particle energy spectra and the auroral emission, at various stages of polar substorm activities. Three vehicles, S-310JA-8, -9 and -10, with the same instruments, carried out the observation up to about 200 km after the nose-cone jettison at around 70 km in altitude.

The payload construction of scientific instruments is illustrated in Fig. 1, and the detailed descriptions for each instrument are as follows.

(a) VAT: visible auroral television camera

The auroral images were taken every 5.62 s by an auroral television camera (VAT) in a visible range from about 400 to 800 nm, a dynamic range being from the equivalent emission rate of about 0.2 to 100 kR at 557.7 nm. A charge couple device (CCD) with an image intensifier was used as an image detector, whose array was 400 (H: horizontal) by 500 (V: vertical). 4×4 pixels were added to make one point of the transmitted picture which consists of 100 (H) \times 101 (V) array. An FOV (field of view) of this image was $53.4^\circ(\text{H}) \times 33.9^\circ(\text{V})$, the absolute value of emission intensity at the center of which was monitored by a photometer (PHO). The photometer had an FOV of 10.8° , a sensitivity of about 10 R, a maximum range of 100 kR, a time resolution of 110 Hz, and an interference filter of 427.8 ± 1.5 nm (for N_2^+ , 1 NG) being used.

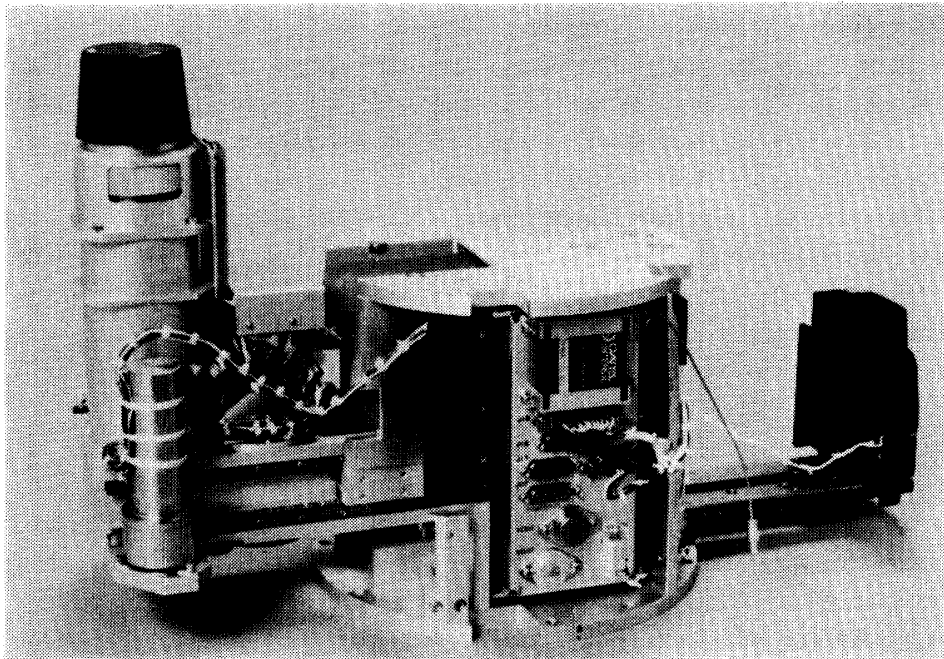


Fig. 2. A photograph of the camera. A counter-balance weight (Wt) is in the right portion of the picture, which keeps the mass center of the camera system on the rocket spin axis.

A camera deployment from the rocket body is shown in Fig. 2. The television picture was taken downwards from the spinning rocket. In order to obtain a still picture, the camera was rotated to compensate for the rocket spin motion by using an angular rate sensor, so as to have the camera view remained unchanged. The shadows of the rocket motor and rear fins can be eliminated by integrating sixteen images over 4.2 s to make one picture, since the shadows rotate with the rocket spin rate of $0.5 \pm$

0.1 Hz. Note that a time of 5.62 s is required for the data transmission telemetry for one picture.

(b) ESP: energy spectrum of particles

Whereas high energy protons precipitate into the high-latitude ionosphere to reveal the so-called proton aurora, the visible auroras are caused mainly by precipitating high energy electrons. A quadri-spherical electrostatic spectrometer was designed to measure energy spectra of electrons for the range from 16 eV to 14.4 keV (in 32 logarithmic steps) with a sweep period of 0.5 s, for three different incident angles of 30°, 90° and 150° with respect to the rocket spin axis. The geometric factors of the spectrometers were $1.78 \times 10^{-4} \text{ cm}^2 \cdot \text{sr} \cdot \text{keV}$ for 90°, and $2.01 \times 10^{-4} \text{ cm}^2 \cdot \text{sr} \cdot \text{keV}$ for 30° and 150° collectors. All three rockets were fired towards the geomagnetic north (313° azimuth from the geographic north at Syowa Station) with a launching elevation of 80°, so as to align the rocket axis parallel to the geomagnetic field line at the ionospheric altitude.

Another analyzer was a magnetic spectrometer to measure the electron flux with four fixed channels, (7.56, 4.13, 1.89 and 0.56 keV for S-310JA-8 and -9, and 18.9, 10.9, 5.26 and 1.44 keV for S-310JA-10). The sensor was placed at the top of the rocket to measure the downwards precipitating electrons nearly parallel to the geomagnetic field line. The data sampling rate was every 20 ms.

(c) NEL: number density of electrons

Energetic electrons lose their energies through collisions with neutral atoms and molecules, and they produce thermal electrons in the ionosphere. A resultant thermal electron density was measured by a sweep-frequency impedance probe with the frequency range up to 10 MHz, a sweep period of 0.5 s, and an applied voltage of 0.1 Vrms. The measured electron density ranged from 10^3 to 10^6 cm^{-3} .

A Langmuir probe (LP) was also installed, and it detected a DC electron current ranging from 10^{-5} to 10^{-7} A, and an AC electron current from 10^{-7} to 10^{-9} A, in order to examine electron density and its fluctuations associated with auroras. LP had a 20 mm spherical electrode, with a fixed applied voltage of +3 V and a frequency response up to 450 Hz.

(d) TEL: temperature of electrons

An electron temperature probe is a kind of resonance probes to detect a change in the floating potential of the electrode with respect to the ambient ionospheric plasma, when a changing ac voltage is applied to the electrode. Electron temperatures were measured with a sampling rate of 0.8 s, and they were in a range from 500 to 4000 K. A floating potential of the rocket was also detected.

(e) Others

To determine particle pitch angles with respect to the geomagnetic field line and the television camera direction in the geographical coordinate system, a three-axis geomagnetic sensor (GA) and a horizon sensor were installed on board the rocket. An electrical programmable timer (EPT) controlled the time sequence of a nose-cone jettison, probe deployments (NEL, LP, TEL), a camera extension (ATV, PHO), and a high tension to ESP. The high tension was turned on at an altitude of about 140 km, in order to avoid an electrical break-down and discharge in the dense atmosphere.

3. Observed Results

3.1. Flight conditions

Three sounding rockets were launched from Syowa Station, Antarctica (invariant latitude= 66.14°S , geomagnetic longitude= 70.98°) at 192701 (UT), on April 4, 1984, into active auroral arcs at a substorm expansion phase, 221410 on May 3, into quiet stable arcs at a pre-breakup phase, and at 231713 on May 28 into a diffuse aurora at a post-break up phase, respectively. The geophysical conditions at each rocket flight have been illustrated and discussed by NAGATA *et al.* (1985), using the ground-based observational data such as the time variations of geomagnetic H -component, the auroral emission intensity at 427.8 nm, 30 kHz VLF hiss intensity, and the cosmic noise absorption (CNA).

A meridian scanning photometer and an all-sky camera at Syowa Station gave the auroral behaviors associated with substorm activities during the rocket flight, which are illustrated in Figs. 3 and 4, together with the rocket trajectories (Fig. 5). Three experiments with S-310JA-8, -9 and -10 are referred to as AURORA I, II and III respectively hereinafter in the text. The seventh picture from the right in the top row was taken at the time of rocket firing, and the rocket burning flare is seen as a spot in the eighth picture. Directions of the picture are such that north is left, south right, west top, and east bottom. From these pictures it is confirmed that AURORA I and II made observation over auroral arcs, whereas AURORA III penetrated into a diffuse aurora. Though these data give a qualitative relationship in position between the rocket and auroras, a detailed examination of the rocket position relative to the changing auroras is to be made with the on board auroral television camera, as discussed later.

The rocket spin rate was designed to be reduced to 0.5 ± 0.1 Hz in the ionosphere with the aid of a Yo-Yo despinner from the initial spin rate of about 3 Hz. The actual values of the spin rate measured by GA and HOS were almost constant during the flight; 0.43, 0.54 and 0.54 Hz for AURORA I, II and III, respectively. The rocket attitude was kept so stable that only one revolution of the precession was observed during the observation periods for the three flights, and this enabled the television camera to take a still picture from the rocket.

3.2. Electron density and temperature

A frequency-swept impedance probe in a plasma detects an upper hybrid resonance, from which the electron density of the plasma can be deduced (OYA, 1965; EJIRI and OYASHI, 1970). The electron density can be obtained also from the dc current to the Langmuir probe (LP). The electron density values deduced from these two independent methods were compared for Aurora I, and this relationship was assumed to hold also for Aurora II when the impedance probe did not operate due probably to a failure in antenna deployment. Figure 6 illustrates the electron density profiles (in a logarithmic scale) obtained by the three rockets during the up-leg. The maximum electron density is observed at the height of 125 km where the ionization produced by isotropic mono-energetic electrons of about 2 keV is the greatest (REES, 1963). On the other hand the particle spectrum in this experiment showed the mono-energetic

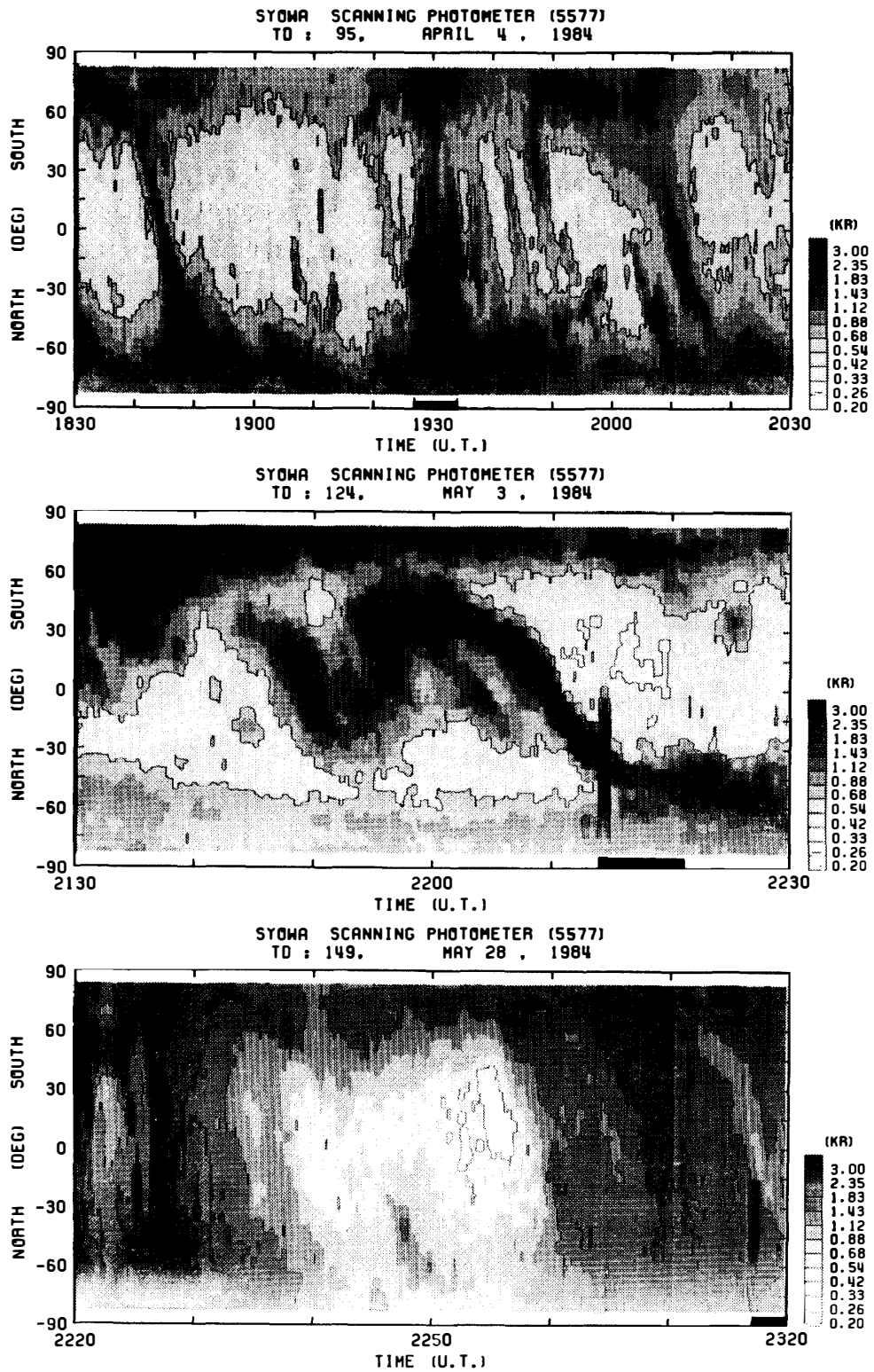
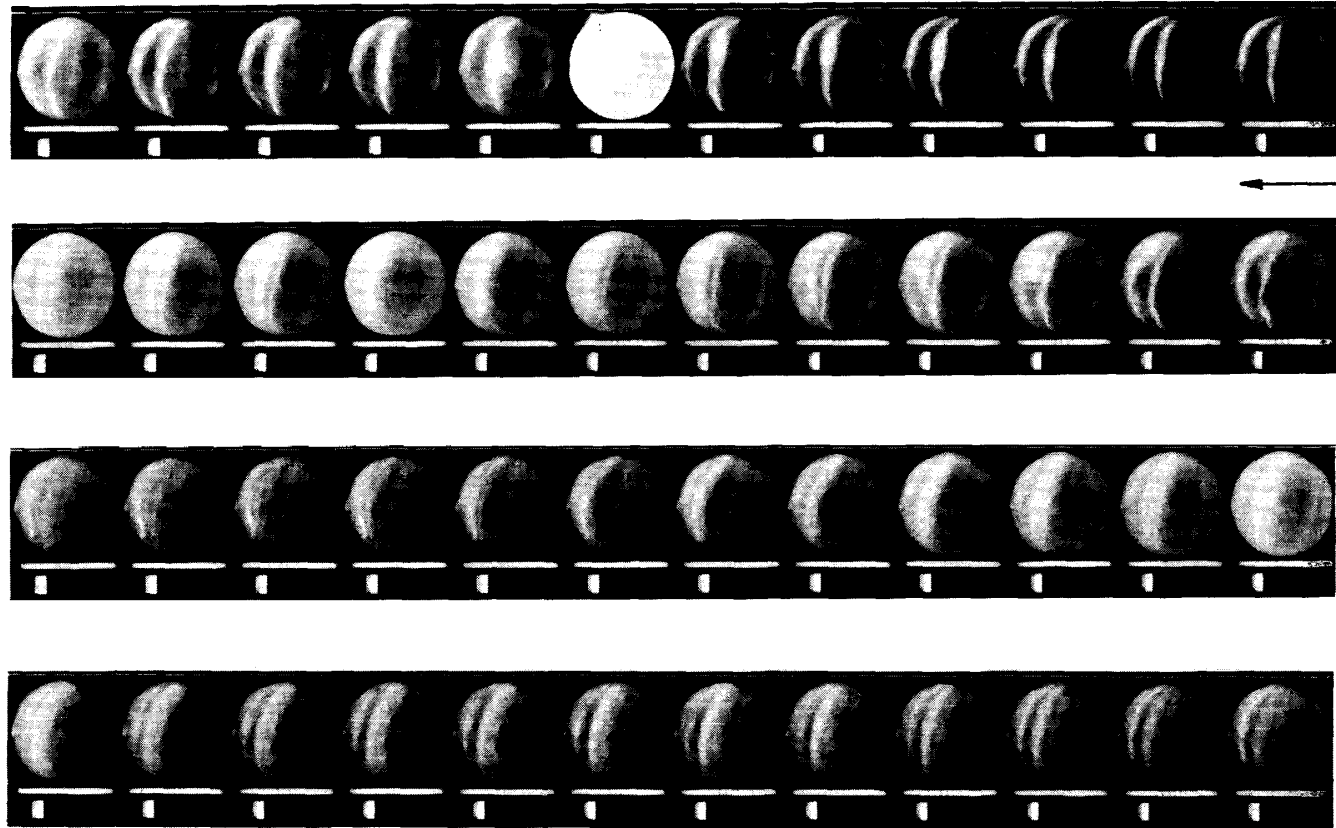


Fig. 3. A meridian-time (UT) display of the scanning photometer which shows the auroral movement in N-S meridian plane. A horizontal bar on the time scale indicates the rocket flight period: (a), (b) and (c) corresponds to AURORA I, II and III, respectively.

ALL-SKY FILM DISPLAY DURING S-310JA-8 FLIGHT



Auroral Images and Particles

Fig. 4. Time-sequential photographs by an all-sky camera at Syowa Station taken at every 10 s for (a) AURORA I, (b) AURORA II, and every 20 s for (c) AURORA.

Fig. 4a. AURORA I 1984 0404 192701 UT = X
 26^m00^s - 34^m10^s at every 10^s



ALL-SKY FILM DISPLAY DURING S-310JA-9 FLIGHT

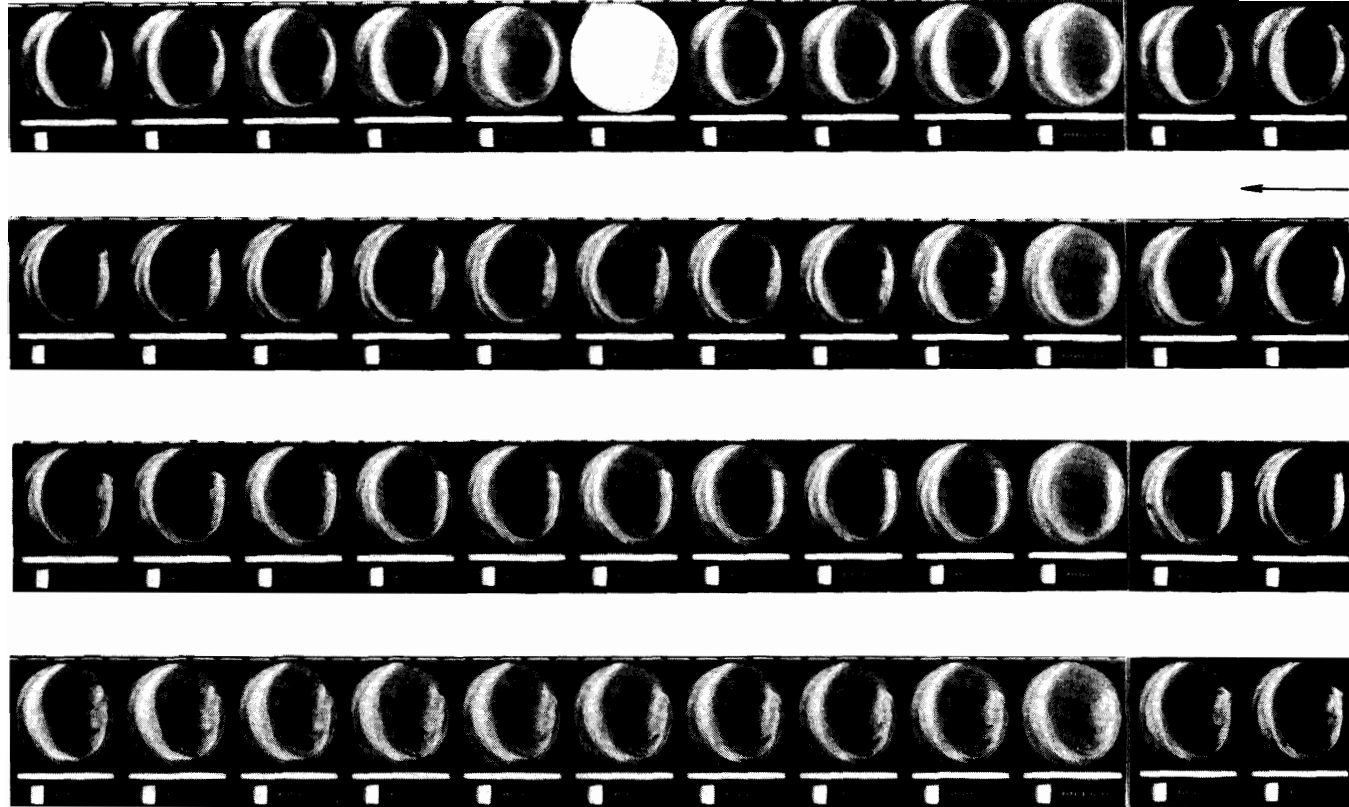
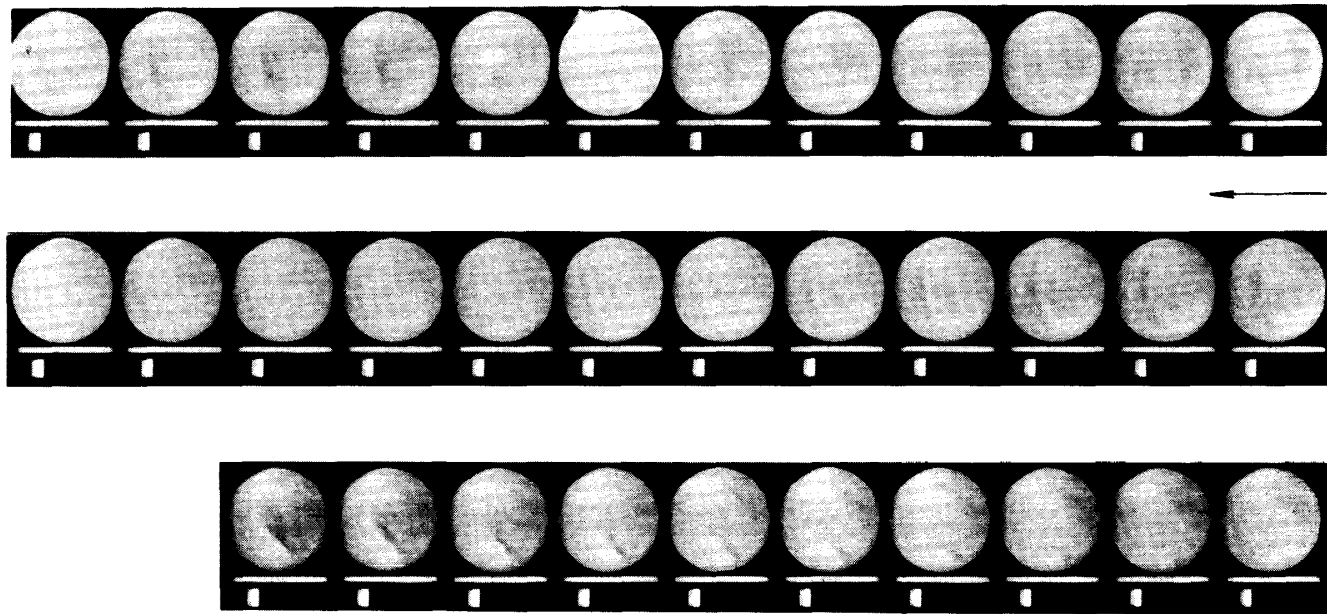


Fig. 4b. AURORA II 1984 0503 221410 UT = x
13^m10^s - 21^m20^s at every 10^s



ALL SKY FILM DISPLAY DURING S-310JA-10 FRIGHT



Auroral Images and Particles

Fig. 4c. AURORA III 1984 0528 231713 UT = x
15^m00^s - 26^m00^s at every 20^s

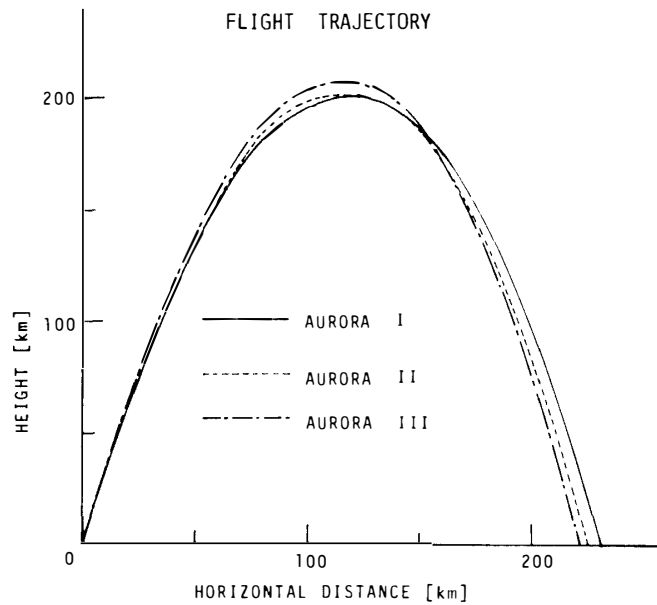


Fig. 5. Three rocket trajectories in horizontal-vertical coordinates.

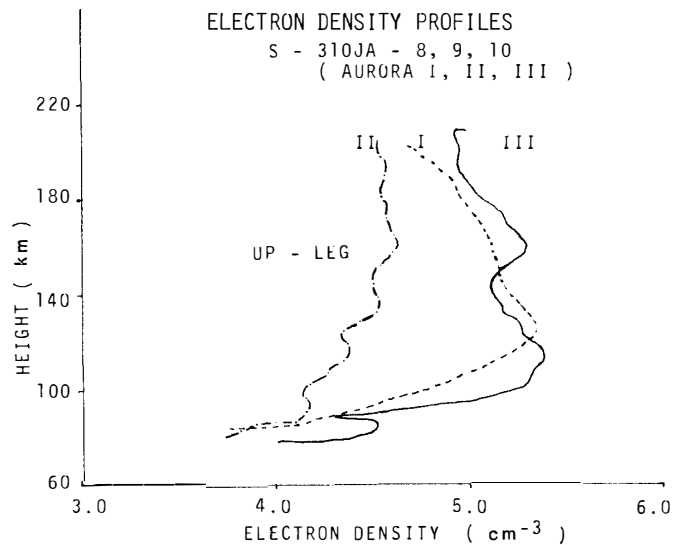


Fig. 6. Electron density profiles for three rockets during their ascent. The abscissa is in a logarithmic scale.

peak at greater than 7 keV. Re-examinations of the interactions between the high-latitude neutral atmosphere and energetic particles including their scattering processes are required. Both the electron density and auroral emission intensity (as discussed later) for AURORA II are less than those for AURORA I. On the contrary, the electron density for AURORA III *i.e.*, diffuse auroras, showed very high values comparable with those for AURORA I, while the auroral emission intensity was less than those for AURORA I. Furthermore, an enhancement in the electron density below the *E* region (down to 80 km) is noticeable in AURORA III. These characteristics of elec-

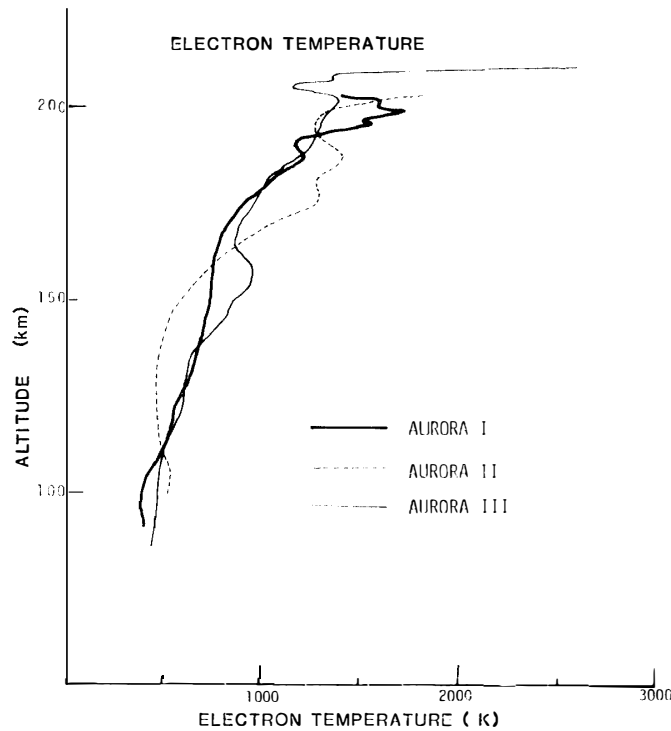


Fig. 7. Electron temperature profiles for three rockets during their ascent.

tron density profiles for different types of aurora are due to a difference in the energy spectra of incident particles.

The electron temperature profiles are illustrated in Fig. 7. Gross features of these results are almost similar to those obtained by various rocket experiments carried out at Syowa Station (OYAMA and HIRAO, 1981). The electron temperature values for AURORA II are less than those for AURORA I and III below about 160 km in altitude, and above this height up to about 175 km this relation is reversed. A rapid change in electron temperature was observed above 150 km, especially for AURORA I. Contrary to PRIMDAHL *et al.* (1984) who reported that both electron density and temperature increase associated with particle precipitation, the result of AURORA I shows that the electron density decreased in the region where the electron temperature increased.

3.3. Energy spectra of auroral electrons

The characteristics of energy spectrum of precipitating energetic electrons for three different types of aurora have been clarified in this experiment (NAGATA *et al.*, 1985). Figure 8 shows the examples of the results for three channels of the quadri-spherical electrostatic analyzer. Three detector channels with 30° , 90° and 150° collimation angles are respectively for precipitating, trapped, and upwards (back-scattered) electrons, because the spin axis was almost aligned along the geomagnetic field line.

As for AURORA I and II (Figs. 8a and 8b), precipitating and trapped particles have a mono-energetic component which has been interpreted as a result of particle accelerations and one of main characteristics of auroral electrons in the inverted-V events observed above auroral arcs. It is noticeable that the trapped flux is more than

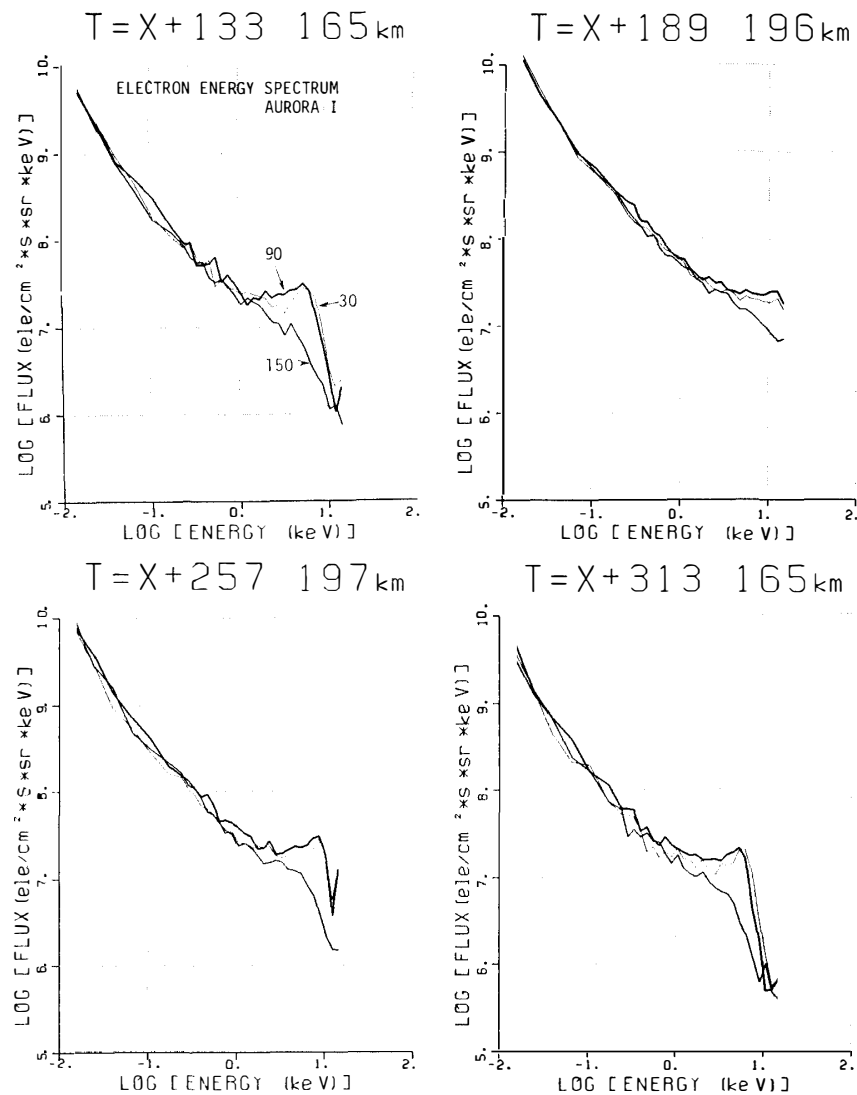


Fig. 8a. AURORA I.

Fig. 8. Examples of energy spectrum of auroral electrons observed by (a) AURORA I, (b) AURORA II and (c) AURORA III, respectively. The ordinate is the electron differential energy flux in log (electrons/cm²·s·sr·keV), and the abscissa is the electron energy in log (energy in keV). Particle pitch angles are indicated in degree, see text.

the precipitating flux in an energy range below the monochromatic peak energy. This distinctive character is also persistent in the case of AURORA III above 200 km in altitude. In contrast to precipitating and trapped electrons, upward electron fluxes have no monochromatic component. Figure 9 elucidates the change in monochromatic peak energy during the flight, namely that higher mono-energetic electrons lead to the brighter auroral arcs at the substorm expansion phase, that electrons for stable arcs prior to the substorm onset (AURORA II) also exhibit an inverted-V type spectrum with energies by one order of magnitude less than the case of AURORA I, and that even in the diffuse aurora in the recovery phase (AURORA III) is a monochromatic peak around 0.5 keV above 200 km in altitude, which is a stopping height of penetrating electrons with energy of about 0.5 keV (REES, 1963). Diffuse auroras are

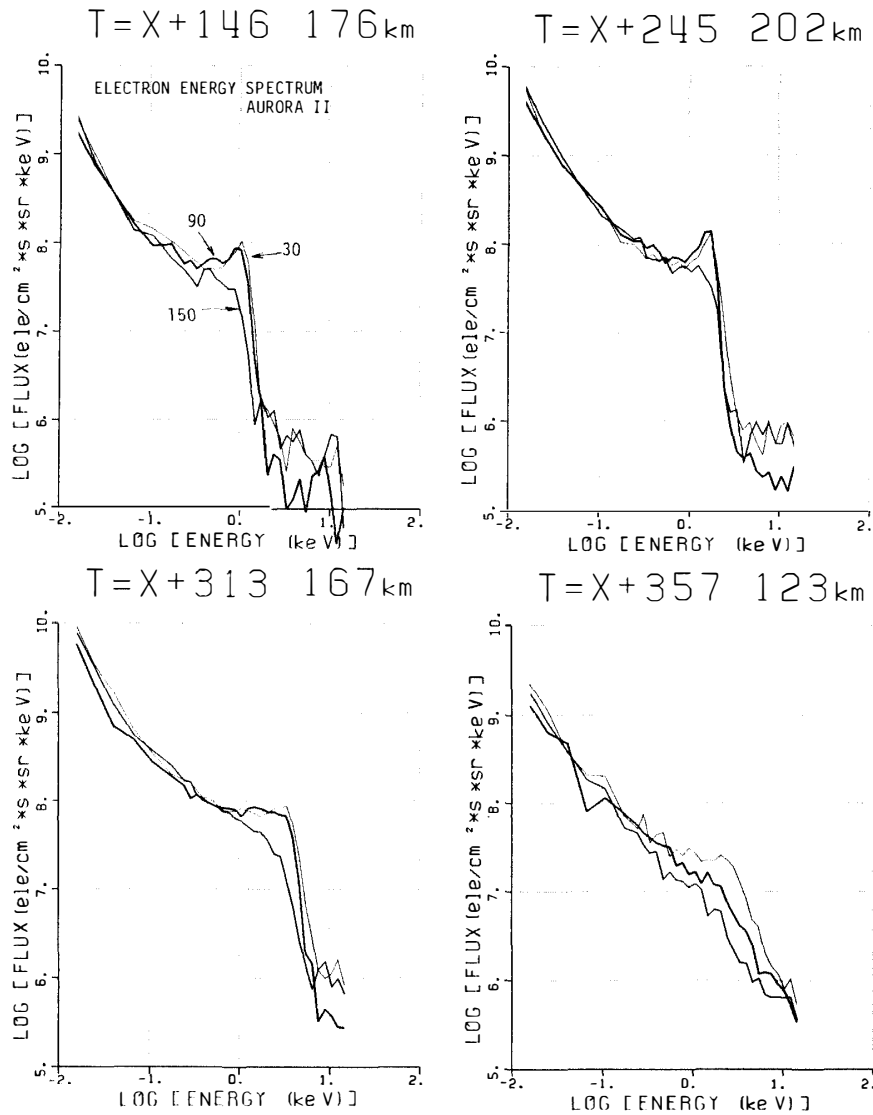


Fig. 8b. AURORA II.

generally produced by electrons with a power-law energy spectrum, when the electron flux is proportional to $E^{-\gamma}$ (E is an electron energy and γ a constant) as illustrated in Fig. 8c.

The gross features of electron energy spectra during the three flights are displayed in an energy-time ($E-t$) spectrogram (Fig. 10). The color code indicated on the right side is proportional to the particle counting rate in particles/cm²·s·sr. This presentation makes it easy to compare the change in particle energy spectrum with time and spatial variations of auroral emissions. Though some particle energy spectra in Fig. 8 show a monochromatic peak, no clear inverted-V shape appears in this $E-t$ spectrograms in Fig. 10. A previous paper by NAGATA *et al.* (1985) reported one example of spectrum change across a stable arc (AURORA II) around $X+234$ s and $X+291$ s. This observed fact is clearly understood by comparing the $E-t$ spectrum and the auroral photoemission rate shown in Fig. 12 for the case of AURORA II. The rocket was entering an auroral arc around $X+260$ s and stayed over the arc for several tens of

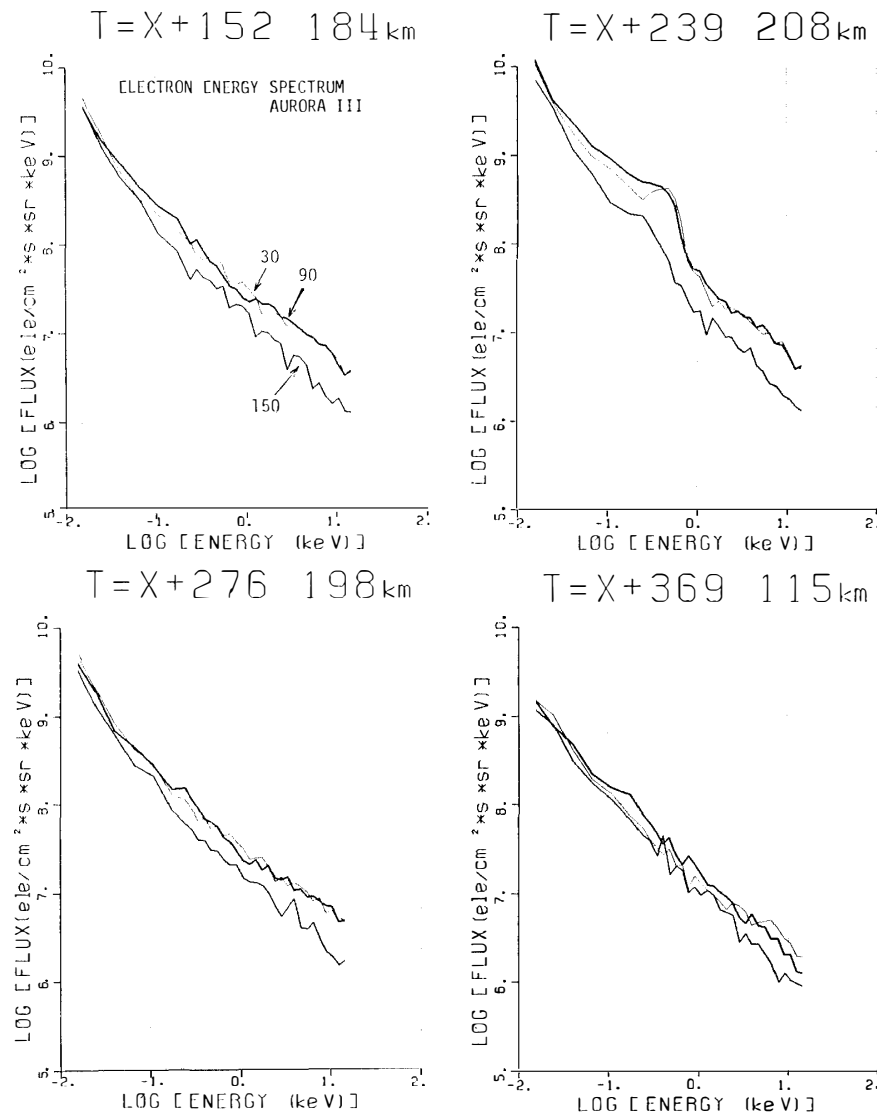


Fig. 8c. AURORA III.

second, during which the enhancements in electron precipitation and a change in energy spectrum took place, as is evident in Fig. 10.

Particle acceleration mechanisms and relevant parallel electric field configurations which might be formed in the near-earth magnetosphere have to be investigated in order to interpret these observational results, but they are beyond the scope of this paper.

3.4. Auroral images and photoemission rates

The onboard auroral television camera took a picture downwards from the rocket in a visible wavelength. Using the aspectmeters (GA and HOS) and the reference signals giving the direction of television screen relative to the rocket body, the geomagnetic direction of the screen was computed. For each flight, we selected 8 pictures out of 60 for illustration in Fig. 11, which show standard behaviors of active auroral arcs, stable arcs, and diffuse auroras encountered in our rocket experiments.

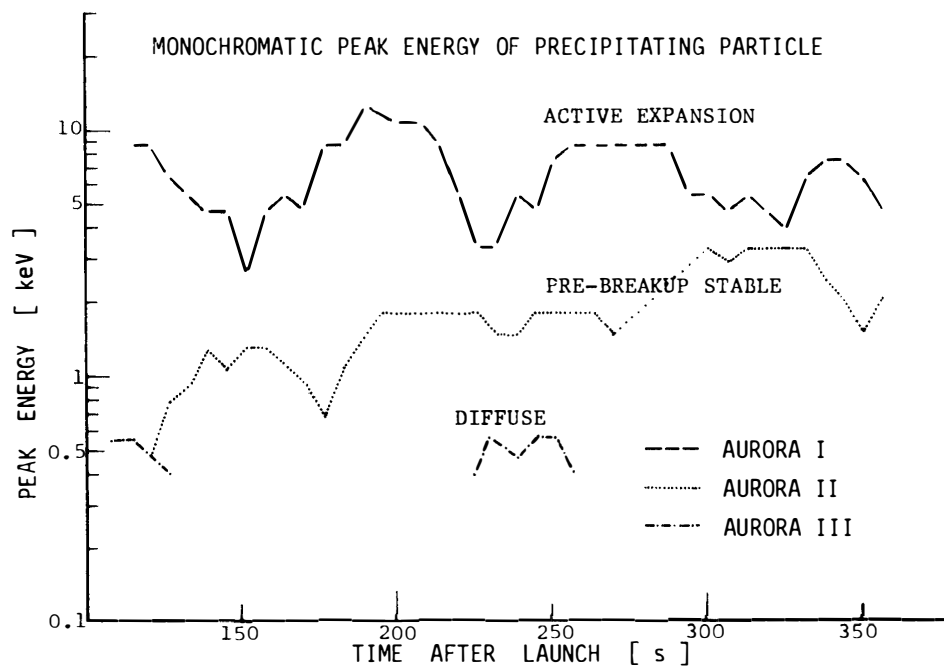


Fig. 9. The monochromatic peak energy of precipitating electrons during the flight.

As for AURORA I, the rocket first encountered an auroral arc at about 84 s after launch, where the horizontal distance from Syowa Station was 40 km north and the altitude was 115 km. It is difficult from Fig. 12 to know whether the rocket crossed over several arcs or the emission intensity varied with time. However, by examining the time-sequential pictures it is concluded that the rocket stayed over the same auroral arc which changed its emission intensity during the time interval from 84 to 240 s. The precipitating particle flux variations with time have been discussed in the previous section. It is necessary to determine a precise position of the foot point of the geomagnetic field line passing through the rocket in order to study the relationship between auroral emissions and auroral particles.

AURORA II observed a weak auroral arc, which was very stable in position, even though the intensity of the photoemission changed. Within the arc a bright patch seemed to travel along the arc from west to east with a velocity of about 1.2 km/s at 110 km height. If the velocity is determined by $E \times B$ motion, the electric field of 53 mV/m is deduced.

The photographs of the ground based all-sky camera (Fig. 4c) show a diffuse aurora which covered over the sky during AURORA III experiment. The onboard auroral television camera revealed fine patchy structures of the diffuse aurora. There is one patch traveling at the edge of aurora from west to east. As shown in Fig. 12, the photoemission rate for this diffuse aurora is very stable during the flight.

Auroral emission spectrum strongly depends on the auroral particle energy spectrum. The ratio of apparent emission rate of different wave lengths, λ_1 and λ_2 for precipitating monoenergetic electrons with energy E is defined as

$$\eta(E, \lambda_1, \lambda_2) = I(\lambda_1)/I(\lambda_2).$$

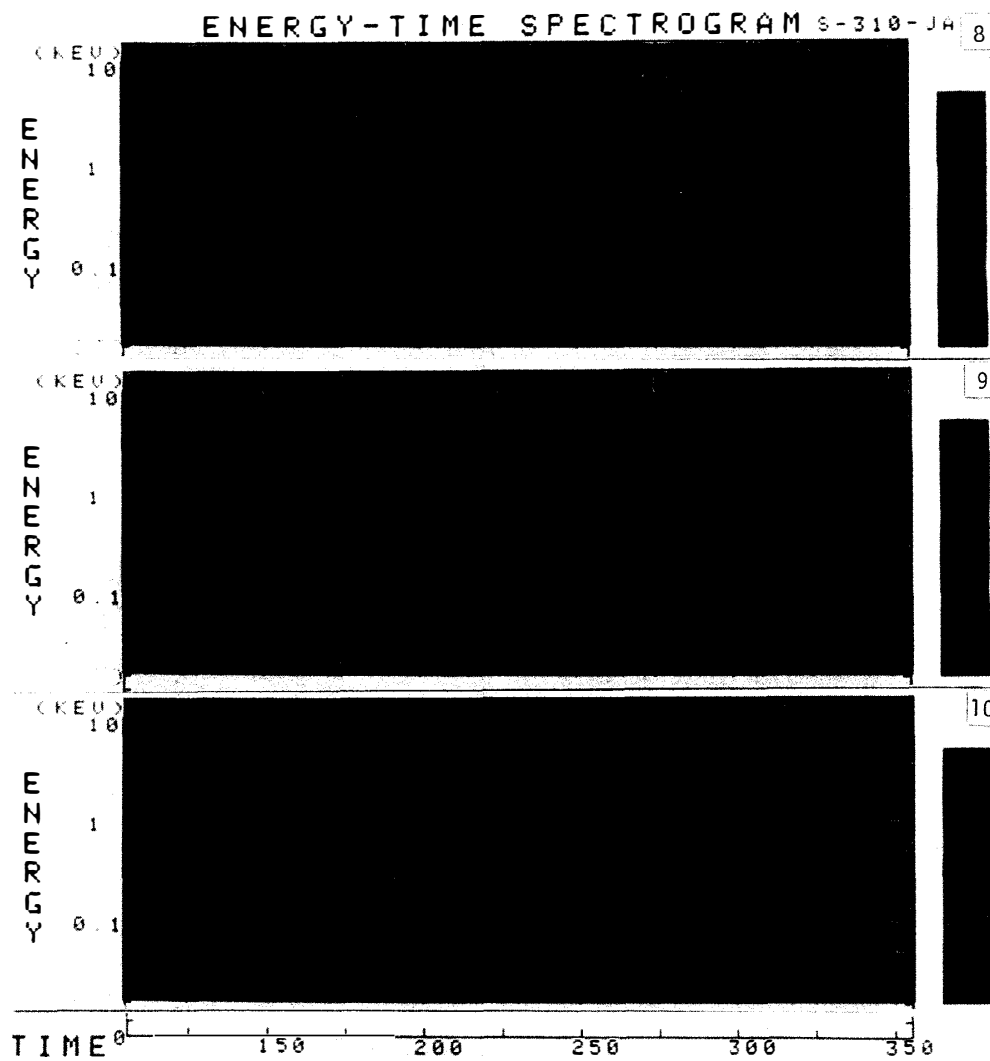


Fig. 10. Energy-time spectrograms of auroral electrons observed by S-310 JA-8, -9 and -10 rockets.

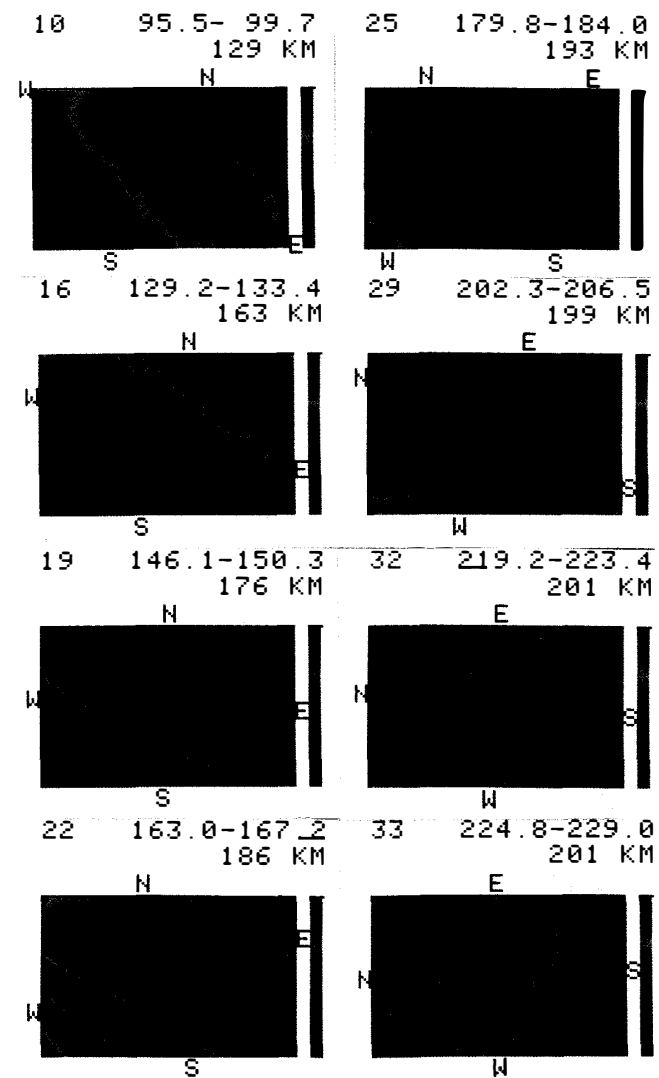


Fig. 11a. AURORA I.

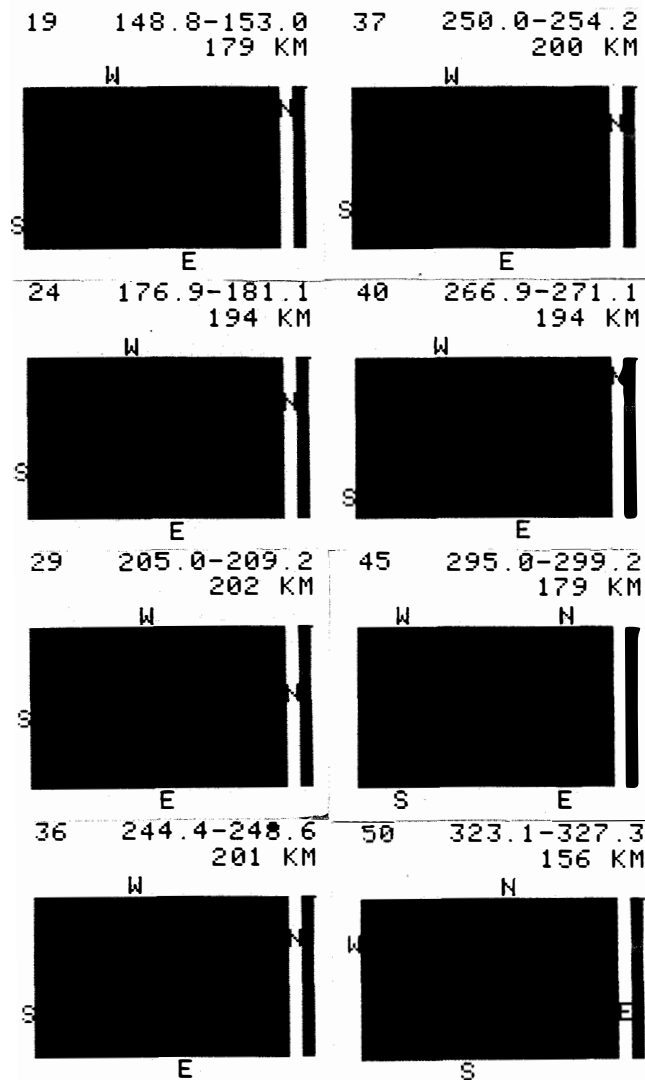


Fig. 11b.
AURORA II.

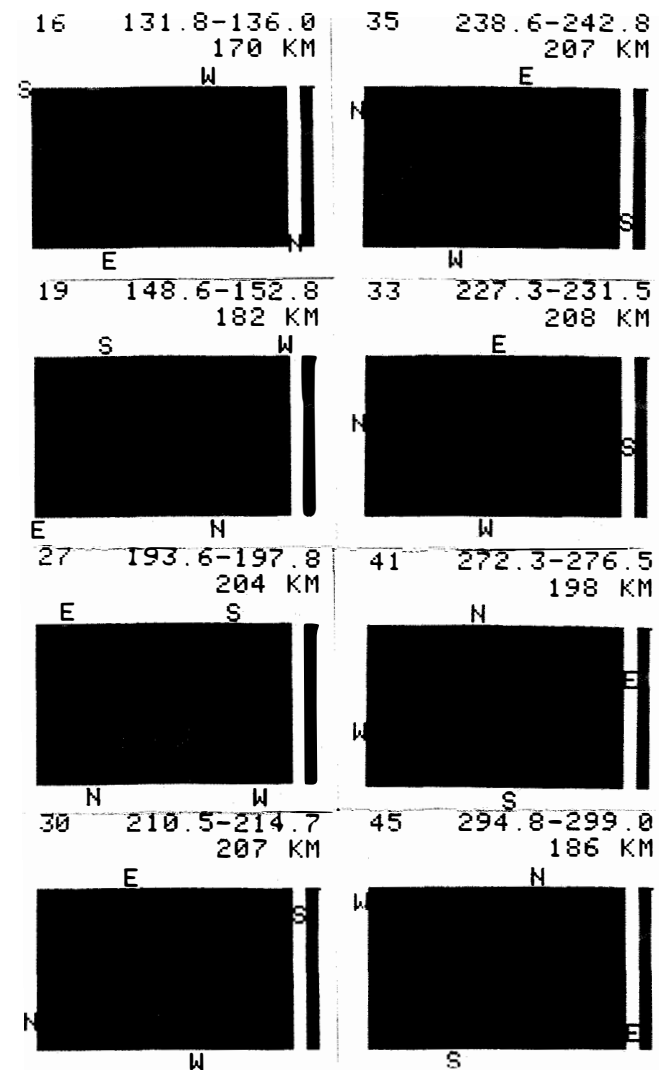


Fig. 11c.
AURORA III.

Fig. 11. False-color displays of auroral images. A number at the top left corner is a sequence number of the picture, followed by the exposure time interval in second after the launch and the rocket altitude. N indicates the geomagnetic north direction from the center of the picture, E east, S south and W west.

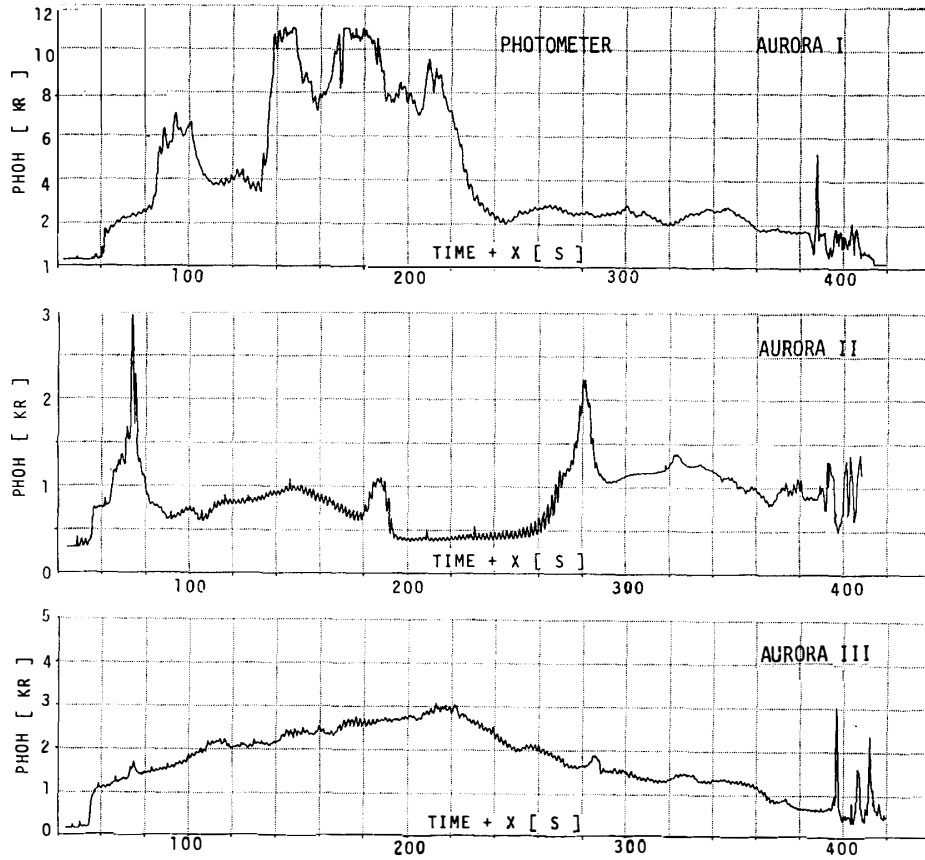


Fig. 12. Auroral photoemission rate measured by PHO.

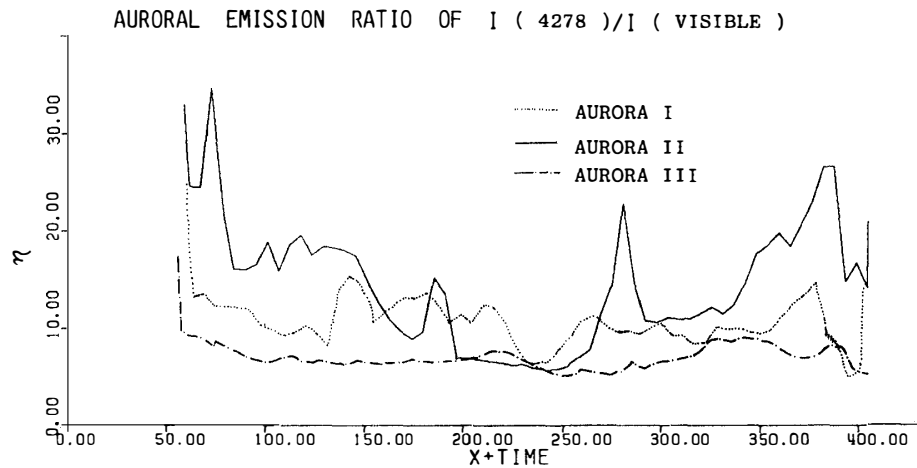


Fig. 13. Ratio of auroral photoemission rate at 427.8 nm and the integrated illuminance over the visible range from 400 to 800 nm for the same area of the FOV of 10.8°.

According to the result of model calculation by JONES (1975) applied to the aurora with an intensity less than 10 kR,

$$\eta(E_1) > \eta(E_2) \quad \text{for } E_1 > E_2,$$

in the case of $\lambda_1 = 427.8$ nm and $\lambda_2 = OI: 557.7$ nm or 630–636.4 nm multiplets. Here η is redefined as (arbitrary unit),

$$\eta = I(427.8 \text{ nm})/I(\text{visible}),$$

where $I(427.8 \text{ nm})$ is an apparent emission rate measured by PHO and $I(\text{visible})$ is an illuminance by VAT. Figure 13 illustrates three cases of η for the three different types of aurora. Though it is impossible to compare the observed value with a simple model calculation, it is understood from Fig. 13, combined with Fig. 10, that a variability of η suggests a difference in particle energy spectrum. From Fig. 9, both AURORA I and II have monoenergetic components, with greater energies for AURORA I than for AURORA II. On the contrary, the value η for AURORA I is less than that for AURORA II during most of the rocket flight. This implies that the active auroral arcs and the stable arcs have quite different relative spectra of auroral emission with respect to the wavelength, though both of these are produced by precipitating electrons with a similar inverted-V type energy spectrum. From Fig. 13 together with Fig. 12, a general relationship seems to hold that the values of η increase substantially as the apparent emission rate increases. The diffuse aurora (AURORA III) has a power-law spectrum with no distinct monoenergetic peak and shows lower values of η than the others.

4. Conclusion

Three sounding rocket experiments have been carried out to investigate the causality between precipitating auroral particles (electrons) and auroral photoemissions. Three different types of aurora, *i.e.*, an active auroral arc at the substorm expansion phase, a stable arc prior to the substorm onset, and a diffuse aurora during the recovery phase, have their own characteristics in the observed electron density and temperature profiles, energy spectra of precipitating, trapped and upward (back-scattered) electrons, auroral images and their apparent emission rates. Time sequential pictures of two dimensional auroral image taken downwards from the rocket enable us to distinguish time and spatial changes of aurora. It is suggested from three different energy spectra of auroral electrons that various mechanisms are operative in the magnetosphere to produce aurora in association with the development and decay in substorm activity.

This study reveals the differences in the above-mentioned observed quantities for the three standard auroras, and gives some qualitative explanations. Although quantitative analyses of the obtained data are yet to be made, these data set will be useful to check some existing theories and for a quantitative establishment of the physical processes of ionization and excitation associated with auroral emissions produced by precipitating energetic electrons from the magnetosphere into the high-latitude upper atmosphere.

Acknowledgments

The S-310JA-8, -9 and -10 rockets were launched during the 25th Japanese Antarctic Research Expedition with the collaboration of Messrs. S. TAKEUCHI, Y. YAMAGAMI, S. ASHIDA and T. TOBASHIRA. The authors wish to thank Profs. T. NAGATA and I. KIMURA for their continuous support and encouragement to this project.

Thanks are also due to Drs. K. HAYASHI and N. YAJIMA for their contributions to the auroral TV system design, to Drs. H. MATSUMOTO, N. KAYA, T. MUKAI, H. MIYAOKA and Mr. H. YAMAGISHI for particle detectors, and to Drs. T. TAKAHASHI and K. OYAMA for electron density and temperature measurements. Data analysis at the Information Processing Center, NIPR, by Messrs. H. SAKURAI and H. OKAMURA were helpful and essential to complete this research.

References

- AKASOFU, S.-I. and KAN, J. R. (1981): *Physics of Auroral Arc Formation*. Washington, D.C., Am. Geophys. Union, 465 p. (Geophys. Monogr. 25).
- ARNOLDY, R. L. and CHOY, L. W. (1973): Auroral electrons of energy less than 1 keV observed at rocket altitudes. *J. Geophys. Res.*, **78**, 2187–2200.
- ARNOLDY, R. L., LEWIS, P. B. and ISAACSON, P. O. (1974): Field-aligned auroral electron fluxes. *J. Geophys. Res.*, **79**, 4208–4221.
- EJIRI, M. and OBAYASHI, T. (1970): Measurement of ionosphere by the gyro-plasma probe. *Rep. Ionos. Space Res. Jpn.*, **24**, 1–12.
- FRANK, L. A. and ACKERSON, K. L. (1971): Observations of charged particle precipitation into the auroral zone. *J. Geophys. Res.*, **76**, 3612–3643.
- HEIKKILA, W. J. (1970): Satellite observations of soft particle fluxes in the auroral zone. *Nature*, **225**, 369–370.
- HOFFMAN, R. A. (1969): Low-energy electron precipitation at high latitudes. *J. Geophys. Res.*, **74**, 2425–2432.
- HOFFMAN, R. A. and EVANS, D. S. (1968): Field-aligned electron bursts at high latitudes observed by OGO 4. *J. Geophys. Res.*, **73**, 6201–6214.
- HOFFMAN, R. A. and LIN, C. S. (1981): Study of inverted-V auroral precipitation events. *Physics of Auroral Arc Formation*, ed. by S.-I. AKASOFU and J. R. KAN. Washington, D.C., Am. Geophys. Union, 80–90 (Geophys. Monogr. 25).
- JONES, A. V. (1975): A model for the excitation of electron aurora and some applications. *Can. J. Phys.*, **53**, 2267–2284.
- LIN, C. S. and HOFFMAN, R. A. (1979a): Characteristics of the inverted-V event. *J. Geophys. Res.*, **84**, 1514–1524.
- LIN, C. S. and HOFFMAN, R. A. (1979b): Fluctuations of inverted V electron fluxes. *J. Geophys. Res.*, **84**, 6547–6553.
- LIN, C. S. and HOFFMAN, R. A. (1982): Narrow bursts of intense electron precipitation fluxes within inverted-V events. *Geophys. Res. Lett.*, **9**, 211–214.
- LOTKO, W. (1986): Diffusive acceleration of auroral primaries. *J. Geophys. Res.*, **91**, 191–203.
- MENIETTI, J. D. and BURCH, J. L. (1981): A satellite investigation of energy flux and inferred potential drop in auroral electron energy spectra. *Geophys. Res. Lett.*, **8**, 1095–1098.
- NAGATA, T., HIRASAWA, T., EJIRI, M. and ONO, T. (1985): Preliminary report on the results of rocket experiments at Syowa Station in 1984. *Mem. Natl Inst. Polar Res., Spec. Issue*, **38**, 128–137.
- OYA, H. (1965): Effect of resonances on the admittance of an RF plasma probe surround by an ion sheath. *Rep. Ionos. Space Res. Jpn.*, **19**, 243–271.
- OYAMA, K.-I. and HIRAO, K. (1981): Gross features of electron temperature profile of polar ionosphere. *Mem. Natl Inst. Polar Res., Spec. Issue*, **18**, 330–334.
- PRIMDAHL, F., BAHNSEN, A., EJIRI, M., HØEG, P., MARKLUND, G., MÆHLUM, B. N., OLESEN, J. K., UNGSTRUP, E. and ZANETTI, L. J. (1984): Rocket-borne and groundbased observations of coincident field-aligned currents, electron beams, and plasma density enhancements in the afternoon auroral oval. *Planet. Space Sci.*, **32**, 561–583.
- PULLIAM, D. M., ANDERSON, H. R., STAMNES, K. and REES, M. H. (1981): Auroral electron acceleration and atmospheric interactions: (1) rocket-borne observations and (2) scattering calcula-

- tions. *J. Geophys. Res.*, **86**, 2397–2404.
- REES, M. H. (1963): Auroral ionization and excitation by incident energetic electrons. *Planet. Space Sci.*, **11**, 1209–1218.
- STASIEWICZ, K. (1985): The influence of a turbulent region on the flux of auroral electrons. *Planet. Space Sci.*, **33**, 591–596.
- THIEMAN, J. R. and HOFFMAN, R. A. (1985): Determination of inverted-V stability from Dynamics Explorer satellite data. *J. Geophys. Res.*, **90**, 3511–3516.

(Received September 30, 1986; Revised manuscript received November 11, 1986)